Structure, dynamics, and thermodynamics of benzene-Ar_n clusters ($1 \leqslant n \leqslant 8$ and $n=19$)

Andreas Dullweber, Matt P. Hodges, and David J. Wales[a)]
University Chemical Laboratories, Lensfield Road, Cambridge CB2 1EW, United Kingdom

(Received 1 July 1996; accepted 16 September 1996)

We use a combination of molecular dynamics, Monte Carlo and geometry optimisation techniques to study benzene-Ar_n clusters for $1 \leqslant n \leqslant 19$, with particular emphasis on $BzAr_{19}$. In particular, we discuss the difficulties which arise in the accurate simulation of heterogeneous clusters due to problems of ergodicity and nonadditive contributions to the energy. The sensitivity of minima, transition states and reaction pathways to parameters of the potential and the induction energy is also considered. An efficient integration scheme with adaptive step size due to Bulirsch and Stoer is employed in the molecular dynamics simulations. Both geometry optimisation and molecular dynamics are considered to evaluate the usefulness of the Jump–walking Monte Carlo method proposed by Frantz, Freeman, and Doll. This approach improves the ergodicity of canonical simulations using data from different temperatures which we achieved using multiple parallel runs. We then apply a multiple histogram method to calculate the relative number of states in phase space and various thermodynamic properties covering the full temperature range in the canonical and the microcanonical ensembles. The Monte Carlo and molecular dynamics simulations result in a consistent picture of transitions between minima and escape times. Finally, we consider the rate of side-crossing by Ar atoms in $BzAr_1$ and $BzAr_{19}$ and compare statistical theories with rates obtained from simulations. © *1997 American Institute of Physics.* [S0021-9606(97)51647-8]

I. INTRODUCTION

Finite, heterogeneous Van der Waals complexes consisting of an aromatic molecule and rare gas atoms have been the subject of numerous studies, both theoretical[1–11] and experimental.[1,3,5,12] However, difficulties arise in comparison between these studies due to uncertainties in the mechanism of formation, energy distribution and stability of the clusters.[4,5] In this work we model the intermolecular interactions of BzAr clusters using a combination of atom–atom dispersion–repulsion, distributed multipoles[13,14] and polarisabilities. We show how the relative importance of terms in the energy varies with the number of Ar atoms and find that the minimum energy and transition state structures are largely unaffected by different sets of model parameters, at least in terms of their geometries. However, the energetic ordering of the minima is sensitive to changes in the potential and we can rationalise this in terms of the specific parameters. In addition, we present a selection of reaction pathways for some of the smaller clusters and compare them with previous suggestions. In our dynamical studies we examine systems at constant temperature (canonical) and at constant energy (microcanonical). Inherent difficulties exist for these simulations due to the complexity of the configuration space. We demonstrate the effect of restricted sampling of configuration space (nonergodicity) for calculating thermodynamic quantities with Monte Carlo methods and how these can be overcome using the Jump–walking proposed by Frantz, Freeman, and Doll.[15] We also use the sampled potential energy distribution in a histogram approach[16,17] to study both the canonical and the microcanonical ensembles. We compare these results with direct microcanonical molecular dynamics simulations to estimate structural transition barriers and escape times.

II. METHOD

A. The intermolecular potential

Atom–atom Lennard-Jones[18] (LJ) parameters (σ and ϵ) are used to describe the dispersion–repulsion interactions, the contribution to the potential energy being summed over each atom of the benzene molecule with each Ar atom, and over all pairs of Ar atoms. The LJ potential is

$$E_{\mathrm{pot}} = 4\epsilon\left[\left(\frac{\sigma}{r}\right)^{12} - \left(\frac{\sigma}{r}\right)^{6}\right] \tag{1}$$

for a given pair of atoms separated by distance r. We test the sensitivity of our results to details of the potential using two sets of parameters for the Ar–Ar, Ar–C and Ar–H interactions as described in Sec. III A.

The charge distribution of the benzene molecule is modelled using distributed multipoles[13,14,19] on each of the C and H atoms. The multipoles have been calculated up to rank 4 (the hexadecapole) following an *ab initio* geometry optimisation which employed 6-311G** (Ref. 20) basis sets with second order Møller-Plesset[21] perturbation theory (MP2) correlation corrections. The first nonvanishing multipole moment is the quadrupole—the molecule is uncharged and according to the point group symmetry, the dipole moment vanishes. The nonzero component of the quadrupole moment transforms as $3z^2 - r^2$ and is expected to make the largest

a)Author to whom correspondence should be addressed.

 0021-9606/97/106(4)/1530/15/$10.00 © 1997 American Institute of Physics

contribution to the electrostatic energy. The first-order electrostatic energy vanishes because the unperturbed Ar atoms have no nonvanishing multipole moments.

For the calculation of higher-order terms in the electrostatic energy (induction), dipole–dipole polarizabilities for benzene and Ar were used in conjunction with the distributed multipoles. We used tabulated polarizabilities for benzene[22] and argon.[23] Induction describes the modification of the permanent multipole moments by the electrostatic fields. Each iteration of the calculation provides an updated set of induced moments. The process is converged when the multipoles no longer change in response to the recalculated fields. Alternatively, a first-order approximation to the induction energy may be obtained from a single iteration of this calculation. The full analysis of these methods is quite lengthy and we refer the reader to Stone's recent publication[19] for a complete description.

Calculating the induction energy is computationally expensive for larger n (especially when we iterate to convergence) and in our more detailed study of $BzAr_{19}$ we neglected this term, as discussed below.

B. Characterization of the potential energy surface

An eigenvector-following technique[24] is used to locate minima and transition states on the potential energy surface (PES). All stationary points are characterised by normal mode analysis using analytic derivatives.[9] Local minima have only real normal mode frequencies, and we follow Murrell and Laidler[25] in defining a true transition state as a stationary point with precisely one imaginary normal mode frequency. Details of the precise algorithms employed in these geometry optimisations and reaction pathway calculations have been given elsewhere[9,26] and numerous previous applications have been described.[9–11,26] Here we simply note that eigenvector-following provides a means to systematically raise the energy for one degree of freedom, while simultaneously minimising in all the conjugate directions. We have implemented eigenvector-following in ORIENT 3.2[27] so that we can suspend both Monte Carlo and molecular dynamics runs at pre-determined intervals, implement a minimisation or transition state search from the instantaneous geometry, and then resume the simulations from where they left off.

C. Monte Carlo simulations

Simulation of the canonical ensemble (constant T, V and N) is commonly performed by the importance sampling scheme of Metropolis *et al.*[28] Monte Carlo (MC) points are in principle independent and could come from very different regions of configuration space as long as they belong to the correct distribution. In contrast to a molecular dynamics trajectory (compare Sec. II D), there is no equation of motion, i.e., no physical time connecting the sampled configurations. Metropolis' algorithm is one efficient way of sampling configuration space in the canonical ensemble. However, the energy-biased random walker is easily trapped in regions of configuration space that are surrounded by broad and high energy barriers. Hence, to improve ergodicity we use the Jump–walking Monte Carlo (JW) approach proposed by Frantz, Freeman, and Doll,[15] as described below.

In JW Monte Carlo a Metropolis walker at lower temperature (hereafter called a ''Jumper'') tries to jump to a distribution generated by a higher temperature run (a ''Diver'') from time to time. In sampling a canonical ensemble the jump acceptance probability $P_{\mathrm{JW}}(x_J \rightarrow x_D)$ to jump from a lower temperature Jumper-configuration, x_J, to a Diver generated configuration, x_D, does not depend only on the energy difference. It also depends on the temperature difference between the Jumper and the Diver ensembles:

$$P_{\mathrm{JW}}(x_J \rightarrow x_D) = \exp\left\{\left(\frac{1}{T_D} - \frac{1}{T_J}\right)[E_{\mathrm{pot}}(x_D) - E_{\mathrm{pot}}(x_J)]\right\}. \tag{2}$$

Hence, in JW simulations both the temperature difference between the Jumper and the Diver runs and the maximum Cartesian displacement are crucial for efficiency.

Tsai and Jordan[29] applied JW to homogeneous clusters. They performed series of simulations decreasing in temperature. Every run stored some of the sampled configurations periodically and the following run was allowed to jump to these with an appropriate probability. Matro, Freeman and Topper[30] have recently developed an implementation which is similar to our approach. They used parallel computing software on multiple processors to realise the communication between individual runs and have applied this technique to study ammonium chloride clusters over a wide temperature range.

We use the Jump–walking idea in a slightly different manner to deal with relatively large systems in ORIENT 3.2.[27] Here the storage of significant parts of the distribution is inconvenient and slow. Instead we perform parallel runs at different temperatures which communicate all the time. To prevent correlation effects, i.e., a Jumper following a Diver closely through configuration space, we use communication buffers between all Jumper/Diver pairs (Fig. 1). Periodically the Diver writes its current configuration at a random position in the buffer which contains many different entries. Hence relatively old configurations can survive in the buffer and correlation is therefore minimized. After a short equilibration time the Jumper is allowed to attempt jumps from time to time to a configuration from the buffer. In practice we start different temperature simulations on one or more computers simultaneously. The highest temperature run only dives, the lowest only jumps, but all the others can both dive and jump to the buffers from the neighboring temperatures. Ergodicity even for the lowest temperature is in principle guaranteed, correlation effects can be minimized and the length of a simulation is no longer restricted by storage problems. Correlation effects due to buffer size, jump probability P_J or dive frequency f_D are easily diagnosed by comparison with standard MC results at a high enough temperature. We will discuss the influence of these parameters below. Here f_D is defined as the number of MC steps taken between storage of the Diver configurations in the buffer. In our simulations of $BzAr_{19}$ the buffer size is fixed at 1000 configurations since

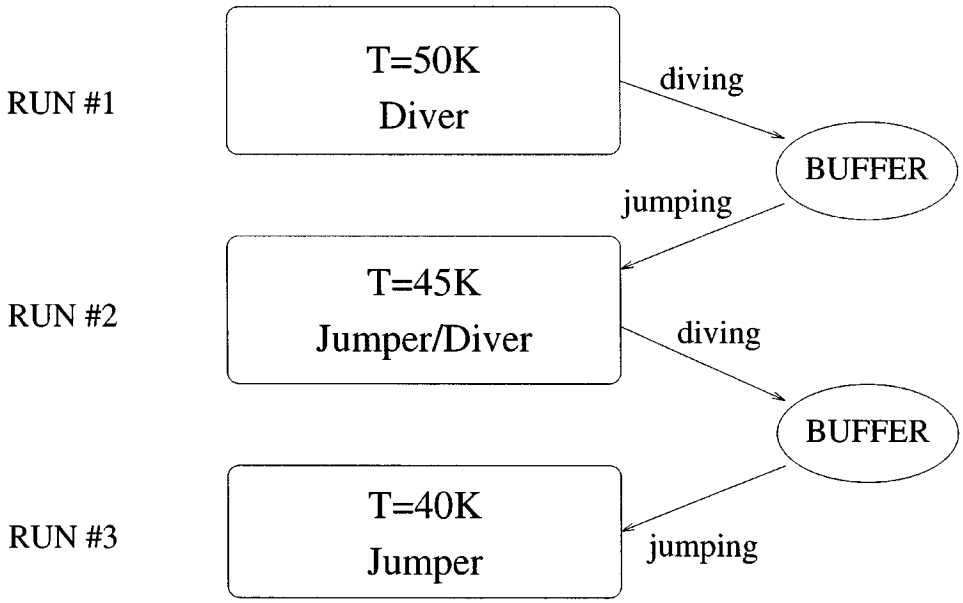

FIG. 1. Schematic of our Jump–walking implementation for a three temperature run. Periodically the Divers write their current configuration at a random position in the appropriate buffer files, whereas the Jumpers, which run simultaneously, attempt jumps from time to time to one of these configurations.

a bigger buffer does not appear to change the results. We fix the constraining spherical container to a radius of 25 bohr. This size should prevent the evaporation and external pressure effects described by Tsai and Jordan.[29] The maximum Cartesian displacement of the standard MC steps was adjusted dynamically to result in an acceptance rate of about 50%.

We can now apply the histogram method proposed by McDonald and Singer[16] and extended by, e.g., Ferrenberg and Swendsen[31,32] and Bichara, Gaspard and Mathieu[33] to calculate thermodynamic properties over a wider temperature range. In our particular MC simulations we generate a normalised histogram $\hat{H}_{T_S}(E_{\rm pot})$ at each sampling temperature T_S. This histogram is equivalent to $P(E_{\rm pot})\delta E_{\rm pot}$,

$$\hat{H}_{T_S}(E_{\rm pot}) \equiv P(E_{\rm pot})\,\delta E_{\rm pot} = \frac{1}{Z_c(T_S)}\,\Omega_c(E_{\rm pot})\,\delta E_{\rm pot} e^{-E_{\rm pot}/kT_S} \tag{3}$$

where $P(E_{\rm pot})\delta E_{\rm pot}$ is the probability of finding the system with a potential energy between $E_{\rm pot}$ and $E_{\rm pot}+\delta E_{\rm pot}$. Here $\Omega_c(E_{\rm pot})\delta E_{\rm pot}$ is the number of microscopic states in configuration space in the above potential energy interval and

$$Z_c(T_S) = \sum_{E_{\rm pot}} \Omega_c(E_{\rm pot})\,\delta E_{\rm pot} e^{-E_{\rm pot}/kT_S} \tag{4}$$

is the configurational partition function. The probability distribution for a different value of T is calculated from

$$\hat{H}_T(E_{\rm pot}) = \frac{\hat{H}_{T_S}(E_{\rm pot}) e^{-E_{\rm pot}(1/kT - 1/kT_S)}}{\Sigma_{E_{\rm pot}} \hat{H}_{T_S}(E_{\rm pot}) e^{-E_{\rm pot}(1/kT - 1/kT_S)}}. \tag{5}$$

The ensemble average of an observable in configuration space, $\langle O_T^c \rangle$, is then found from

$$\langle O_T^c \rangle = \sum_{E_{\rm pot}} O(E_{\rm pot}) \hat{H}_T(E_{\rm pot}). \tag{6}$$

We will use the above method for observables dependent only on $E_{\rm pot}$, but it can be generalised in a straightforward fashion as discussed below. We normally smoothed the histograms by fitting to an expansion of Gaussians which improves the accuracy especially for the lower energy region. Five Gaussian functions are almost always sufficient in the interpolation procedure. However, systematic errors arise at temperatures very different from T_S because the quality of the histograms is poor far away from the sampled average potential energy.

Various algorithms have been proposed to combine the histogram information gained at different temperatures in a multiple histogram method.[17,29,32–34] We implemented the approach of Weerasinghe and Amar.[17] This technique employs a least-squares fit to find the relative number of configurational states, $\Omega_c(E_{\rm pot})\delta E_{\rm pot}$, which strikes an optimized balance between the estimated configurational densities for each value of T_S. Different statistical weights of the histograms as used by Tsai and Jordan[29] are not taken into account in the present work. We convolute $\Omega_c(E_{\rm pot})\delta E_{\rm pot}$ with the density of kinetic states, $\Omega_k(E_{\rm kin})$, which is known analytically from the volume of the ν-dimensional energy hypersphere in momentum space as

$$\Omega_k(E_{\rm kin}) = \frac{\partial}{\partial E_{\rm kin}} \int_{E_{\rm kin}(p) \leqslant E_{\rm kin}} d^\nu p \propto E_{\rm kin}^{\nu/2-1}. \tag{7}$$

Here ν is the number of degrees of freedom. In our microcanonical molecular dynamics simulations the overall linear and angular momenta are integrals of motion. Hence, for comparison ν is set to $6N_{\rm Bz}+3N_{\rm Ar}-6$ and we obtain

$\Omega(E)\,\delta E$, the number of microscopic states in phase space with total energy between E and $E+\delta E$, from the convolution[34,35]

$$\Omega(E)\,\delta E=\delta E\int_0^E \Omega_k(E')\,\Omega_c(E-E')\,dE'. \tag{8}$$

The different numbers of states are only known up to a multiplicative constant, but all thermodynamical functions of interest can be calculated from the relative values of $\Omega(E)\,\delta E$. We consider for the microcanonical ensemble the entropy,

$$S(E)=k_B\,\ln[\Omega(E)\,\delta E], \tag{9}$$

and the temperature,

$$\frac{1}{T(E)}=\frac{\partial S(E)}{\partial E}, \tag{10}$$

as functions of the total energy. We compare these quantities with the direct molecular dynamics results. For the canonical ensemble we use the canonical partition function,

$$Z(T)=\int e^{S(E)/k_B-E/k_BT}dE, \tag{11}$$

to calculate the canonical internal energy,

$$U(T)=k_BT^2\,\frac{\partial\,\ln Z(T)}{\partial T}, \tag{12}$$

and the canonical heat capacity,

$$C_V(T)=\frac{\partial U(T)}{\partial T}, \tag{13}$$

as functions of temperature. To test the initial Monte Carlo results obtained from the multiple histogram method we also estimate the specific heat from the fluctuations of the potential energy:[29,36,37]

$$C_V(T)=\frac{1}{k_BT^2}\,(\langle E_{\rm pot}^2\rangle-\langle E_{\rm pot}\rangle^2)+\frac{\nu}{2}\,k_B, \tag{14}$$

where the last term represents the kinetic contribution.

We do not show error bars in most of our diagrams. However, all averages of the potential energy are converged to 1% or better and the numerical derivatives and integrals employed are of much higher accuracy. More careful error estimates should include correlation time effects[29] but we have not gone to such lengths in this paper. Correlation between the molecular dynamics integration steps is actually very small because the propagator we use favours rather large time steps.

D. Molecular dynamics simulations

Unfortunately, for a many-particle system like $BzAr_{19}$ rather long trajectories are needed to estimate thermodynamic properties of the microcanonical ensemble (constant E, V and N) using molecular dynamics (MD) with any accuracy. As for Monte Carlo studies simulations are likely to be trapped in isolated regions of the constant energy hyperplane in phase space. However, insurmountable transition states can make simulations restricted to such regions meaningful, but even calculating locally ergodic trajectories can be time consuming.

Our MD integration in ORIENT 3.2[27] is done with an adaptive step size propagator due to Bulirsch and Stoer.[38,39] Here the result for a large integration step is extrapolated from a sequence of finer and finer substep-integrations of the large interval. The extrapolation procedure provides us then with an error estimator for each integration step. This is used for the dynamical adjustment of the step size. Both the chosen propagator and the adaptive step size are designed to minimise the number of force calculations. This strategy is much more efficient then corrector-predictor and static step size schemes. In addition it allows us to directly control the integration quality with regard to the integration variables and the integrals of motion. In our adaptive step size control we consider both the accuracy of the phase space coordinates and the conservation of energy.

In the microcanonical simulations we loop over increasing values of the total energy. At each new energy we start from the last configuration of the previous energy. The initial kinetic energies are equally distributed amongst the vibrational degrees of freedom only but spread out into the internal rotations after a few time steps. The initial centre of mass motion and the overall angular momentum are always corrected so that they vanish at each new energy. These overall momenta are well conserved in the integration since we do not use a constraining container for MD.

All trajectories are monitored and quenched periodically to provide insight into the region of phase space in question. We calculate the kinetic temperature $T_{\rm kin}$ as,

$$T_{\rm kin}=\frac{2\langle E_{\rm kin}\rangle}{(6N_{\rm Bz}+3N_{\rm Ar}-6)k_B}, \tag{15}$$

resulting from the average kinetic energy per degree of freedom.[40] Here conservation of the overall linear and rotational momenta has to be taken into account.

We treat the benzene molecule as a rigid body in all simulations. The orientation space is represented by a Euclidean metric using the corresponding quaternion parameters.[37,41–43] An equivalent angle-axis description[43] is also possible without singularities, in contrast to, e.g., Euler angles. The latter approach is convenient for sampling orientation space in Monte Carlo simulations and we used it in static step size calculations. However, the integration scheme with adaptive step size control is much more convenient in the quaternion representation where larger steps can be taken without problems due to noncommuting finite rotations.

III. RESULTS

A. LJ parameters

1. $BzAr_n$, $1\leqslant n\leqslant 8$

We systematically search the PES's of $BzAr_n$ with $1\leqslant n\leqslant 8$ using two sets of rather different LJ parameters recommended by Ondrechen, Berkovitch-Yellin and Jortner[6] (OBJ) and Schmidt, Le Calvé and Mons[1] (SCM). In particular the SCM Ar–Ar well depth is about 20% larger than that

TABLE I. Lennard-Jones parameters from the OBJ[6] and SCM[1] sources. σ is given in bohr(Å) and ϵ is given in millihartree(cm^{-1}).

	OBJ		SCM	
	σ	ϵ	σ	ϵ
Ar–Ar	6.51	0.379	6.33	0.451
	(3.45)	(83.1)	(3.35)	(99.0)
Ar–C	6.46	0.184	6.46	0.183
	(3.42)	(40.4)	(3.42)	(40.2)
Ar–H	6.07	0.205	6.07	0.150
	(3.21)	(45.0)	(3.21)	(33.0)

used by OBJ and the Ar–H well is about 25% smaller. The equilibrium separations ($2^{1/6}\sigma$) are identical for Ar–C and Ar–H and differ by about 3% for Ar–Ar, i.e., these differences are small compared with the different well depths. These parameters are summarized in Table I.

We now introduce some notation which has been used, e.g., by Schmidt *et al.*, to describe the positions of the Ar atoms with respect to the benzene molecule. Here $(l|m|n)$ signifies that there are l Ar atoms on one side of the ring, n Ar atoms on the other side and m Ar atoms in or very close to the plane of the molecule—the m Ar atoms are referred to as bridging atoms, and we observe such structures as local minima for $BzAr_n$ with $n \geqslant 3$. We note that for structures with no bridging Ar atoms (i.e., $m=0$) the notation may be abbreviated to $(l|n)$, where l and n are defined as above. For

TABLE III. Selected rearrangement mechanisms for some small $BzAr_n$ clusters. We report the energies of the minima (E_{min1} and E_{min2}), the energy of the transition state (E_{ts}), the barrier heights (Δ_1 and Δ_2), and the transition state point groups (PG_{ts}). All energies in millihartree.

n	params	E_{min1}	Δ_1	E_{ts}	PG_{ts}	Δ_2	E_{min2}
1	OBJ	−1.804	0.975	−0.829	C_{2v}	0.975	−1.804
	SCM	−1.605	0.893	−0.712	C_{2v}	0.893	−1.605
2	OBJ	−3.269	0.090	−3.179	C_{2v}	0.090	−3.269
		−3.269	0.145	−3.124	C_{2v}	0.145	−3.269
		−3.269	0.604	−2.666	C_s	0.964	−3.630
		−3.269	1.065	−2.204	C_{2v}	1.065	−3.269
		−3.269	1.487	−1.783	C_s	1.487	−3.269
	SCM	−3.023	0.086	−2.937	C_{2v}	0.086	−3.023
		−3.023	0.115	−2.908	C_{2v}	0.115	−3.023
		−3.023	0.672	−2.351	C_s	0.881	−3.233
		−3.023	0.996	−2.027	C_{2v}	0.996	−3.023
		−3.023	1.379	−1.645	C_s	1.379	−3.023

TABLE II. The energies, in millihartree, and the point groups (PG) for the five lowest $BzAr_n$ minima found with the OBJ and SCM LJ parameters. The labels are fully described within the text.

	OBJ			SCM		
n	Label	PG	E	Label	PG	E
1	$(1_c\|0)$	C_{6v}	−1.804	$(1_c\|0)$	C_{6v}	−1.605
2	$(1_c\|1_c)$	D_{6h}	−3.630	$(1_c\|1_c)$	D_{6h}	−3.232
	$(2_c\|0)$	C_s	−3.269	$(2_c\|0)$	C_s	−3.023
3	$(3_s\|0)$	C_{3v}	−5.150	$(3_s\|0)$	C_{3v}	−4.915
	$(2_c\|1_c)$	C_s	−5.111	$(3_c\|0)$	C_s	−4.891
	$(3_c\|0)$	C_s	−5.108	$(2_c\|1_c)$	C_s	−4.666
	$(3_l\|0)$	C_{2v}	−4.694	$(3_l\|0)$	C_{2v}	−4.410
	$(2_c\|1\|0)$	C_s	−4.503	$(2_c\|1\|0)$	C_s	−4.213
4	$(3_s\|1_c)$	C_{3v}	−7.006	$(4_s\|0)$	C_{2v}	−6.765
	$(3_c\|1_c)$	C_s	−6.966	$(4_c\|0)$	C_s	−6.755
	$(4_s\|0)$	C_{2v}	−6.948	$(3_s\|1_c)$	C_{3v}	−6.571
	$(4_c\|0)$	C_s	−6.936	$(3_c\|1_c)$	C_s	−6.549
	$(2_c\|2_c)$	C_{2v}	−6.640	$(1+3_s\|0)$	C_{3v}	−6.379
5	$(4_s\|1_c)$	C_{2v}	−8.819	$(5_c\|0)$	C_s	−8.626
	$(4_c\|1_c)$	C_s	−8.810	$(5_s\|0)$	C_s	−8.557
	$(5_c\|0)$	C_s	−8.771	$(4_s\|1_c)$	C_{2v}	−8.437
	$(5_s\|0)$	C_s	−8.708	$(4_c\|1_c)$	C_s	−8.429
	$(3_s\|2_c)$	C_s	−8.519	$(1+4_c\|0)$	C_s	−8.402
6	$(5_c\|1_c)$	C_s	−10.66	$(6_c\|0)$	C_s	−10.55
	$(6_c\|0)$	C_s	−10.65	$(6_s\|0)$	C_{3v}	−10.39
	$(5_s\|1_c)$	C_s	−10.60	$(5_c\|1_c)$	C_s	−10.32
	$(6_s\|0)$	C_{3v}	−10.50	$(1+5\|0)$	C_1	−10.29
	$(3_c\|3_c)$	C_{2v}	−10.44	$(1+5_c\|0)$	C_s	−10.26
7	$(7_c\|0)$	C_{6v}	−12.88	$(7_c\|0)$	C_{6v}	−12.89
	$(6_c\|1_c)$	C_s	−12.56	$(2+5\|0)$	C_1	−12.27
	$(6_s\|1_c)$	C_{3v}	−12.40	$(6_c\|1_c)$	C_s	−12.26
	$(3_c\|1\|3_c)$	C_{2v}	−12.34	$(1+6_c\|0)$	C_1	−12.20
	$(4_c\|3_c)$	C_1	−12.32	$(1+6\|0)$	C_s	−12.20
8	$(7_c\|1_c)$	C_{6v}	−14.81	$(7_c\|1_c)$	C_{6v}	−14.62
	$(3_s\|2\|3_s)$	C_{2v}	−14.29	$(1+7_c\|0)_a$	C_s	−14.57
	$(4_c\|1\|3_c)$	C_1	−14.28	$(1+7_c\|0)_b$	C_s	−14.49
	$(4_c\|4_c)$	C_{2v}	−14.27	$(7_c\|1\|0)$	C_s	−14.34
	$(7_c\|1\|0)$	C_s	−14.26	$(7_c\|1\|0)$	C_s	−14.24

example a structure with three Ar atoms on either side of the benzene molecule is labeled (3|3) and if an additional Ar atom is placed in the plane of the molecule this is referred to as a (3|1|3) structure.

Following Schmidt *et al.* we use two additional labels *c* and *s* for describing the arrangement of the Ar atoms with respect to the C_6 axis of the benzene molecule. We use *c* when one of the Ar atoms lies on or close to this axis and *s* when this point is ''shared'' by more than one Ar atom. For *c*-type arrangements of Ar atoms those not above the C_6 axis are positioned with the benzene molecule acting as a template—each atom lies in or near to one of the mirror planes between the H atoms. This leads to closed-packed arrangements of Ar atoms, which we would expect to see up to $BzAr_7$ for one-sided structures, at which point the benzene ring becomes ''saturated.'' We observe *s*-type minima for $BzAr_3$ to $BzAr_6$ and for the transition state $(2_s|0)$ in $BzAr_2$, which connects two permutational isomers of the $(2_c|0)$ local minimum in a degenerate rearrangement in agreement with previous calculations by Wales.[2]

The additional labels *s* and *c* are useful to describe many of the minima that we observe in the smaller $BzAr_n$ clusters because of the influence that the benzene molecule has on the arrangement of the Ar atoms. For two-sided structures it is generally the case that the arrangement of Ar atoms on each side of the molecule is similar to one observed for a one-sided local minimum in a smaller cluster. For example, local minima exist for $(3_c|0)$ and $(2_c|0)$ structures and as indicated in the discussion above we also observe $(3_c|2_c)$ minima. This notation does not indicate the relative orientations of the two sets of Ar atoms and hence several local minima generally exist with the same label in such cases.

The majority of the low-lying local minima for the smaller clusters have pseudo-planar arrangements of Ar atoms on each side of the ring, i.e., each atom is approximately the same perpendicular distance from the plane of the benzene molecule. Some structures have a second plane containing one or two Ar atoms above the first. An example for which three Ar atoms are in an *s*-type arrangement with the fourth acting as a cap would be labelled $(1+3_s|0)$.

This nomenclature allows us to describe many of the local minima that we observe for up to eight Ar atoms. However, for clusters as small as $BzAr_7$ we observe structures not based primarily on the geometry of the benzene molecule and there are local minima with pseudo 5-fold symmetric arrangements of Ar atoms. For $BzAr_{19}$ we see structures based on the neat Ar_{19} double icosahedron as discussed below.

Details of some low-lying minima, along with their point groups and energies, are given in Table II. Details of sample reaction pathways are given in Table III. It is noteworthy that one-sided minima are found for which the expected close-packed arrangement of Ar atoms does not exist, i.e., minima for which the Ar atoms are spread above the benzene molecule in patterns which do not favour the Ar–Ar interactions. We find such structures for $BzAr_n$ with $3 \leqslant n \leqslant 5$ and these, as for the *s*- and *c*-type arrangements, are able to combine with other Ar atoms to form two-sided structures. For example, a minimum with a linear arrangement of Ar atoms above the benzene molecule exists. We label this C_{2v} structure $(3_l|0)$ and have also observed $(3_l|1_c)$. The unfavourable arrangements of Ar atoms in these minima make them relatively weakly bound.

The geometries of the minima and the transition states, calculated without the induction energy contribution, are qualitatively unaffected in almost all cases when we change the LJ parameters from those of OBJ to SCM. Occasionally a structure characterized for one set of LJ parameters as a minimum is not so for the other set and sometimes the connectivity of the minima changes, i.e., which minima are linked by particular transition states. Although the structures generally do not change very much, we find that the energetic ordering of the local minima is rather different, and we observe that the SCM minima show a preference for one-sided structures compared to those of OBJ. The SCM lowest minima for $BzAr_n$ with $3 \leqslant n \leqslant 7$ are all one-sided, with close-packed, pseudo-planar arrangements of Ar atoms. The size of the Ar–Ar well depth accounts for the fact that this trend was not observed for the OBJ lowest energy minima where two-sided structures have greater stability. For example, the $(3_s|0)$ structure is lowest in energy for $BzAr_3$ for both SCM and OBJ but for $BzAr_4$ and $BzAr_5$ the lowest minima found with the SCM parameters are $(4_s|0)$ and $(5_c|0)$ and with the OBJ parameters are $(3_s|1_c)$ and $(4_s|1_c)$, see Table II.

For $BzAr_n$ with $n \geqslant 2$ we see differences in the transition states calculated using the different parameters. For $BzAr_2$ we find five transition states for both OBJ and SCM. Four are degenerate rearrangements of the $(2_c|0)$ minimum and the other is nondegenerate, exchanging the $(2_c|0)$ and the $(1_c|1_c)$ minima. There is a correlation between the energies of the transition states and the number of Ar atoms crossing the benzene ring. The two highest lying transition states involve both Ar atoms crossing the ring and mediate degenerate rearrangements. The next highest transition state is for the nondegenerate rearrangement in which one Ar atom changes sides. The remaining two degenerate rearrangements involve no ring-crossing and in the higher of the two the benzene molecule effectively rotates by 60°, thus changing the site of one of the Ar atoms. The lower of the latter two transition states corresponds to a $(2_s|0)$ structure and the corresponding rearrangement changes the Ar atom lying on the C_6 axis of the molecule. The transition states permute the Ar atoms in the same way for both the OBJ and SCM parameters, and with one exception the rearrangements are equivalent. During the 60° rotation, for the SCM parameters one Ar atom remains on the C_6 axis of the benzene molecule. However, for the OBJ parameters the rotation of the benzene molecule occurs after the $(2_s|0)$ structure has been reached and, therefore, involves a direct connection between two transition states. If we label the $(2_c|0)$ minimum min the $(2_s|0)$ transition state $ts1$ and the second transition state $ts2$, then we can label the two low-lying OBJ pathways as,

$$\text{min} \rightarrow ts1 \rightarrow \text{min}$$

$$\text{min} \rightarrow ts1 \rightarrow ts2 \rightarrow ts1 \rightarrow \text{min},$$

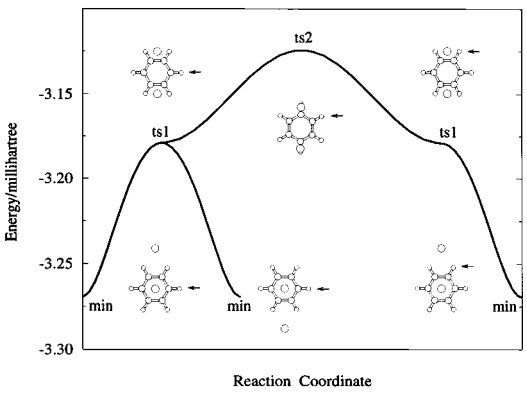

FIG. 2. Two rearrangement pathways for $BzAr_2$ calculated using the OBJ parameters. One includes a direct connection between two transition states. Both pathways are for degenerate rearrangements of the $(2_c|0)$ minimum. The arrows point to the same H atom in all cases, to clarify the relative orientations of the benzene molecule.

though the right hand side minimum is not the same permutational isomer for the two paths (Fig. 2). Branching points must exist between $ts2$ and $ts1$ on both sides of the second path. We find such rearrangements involving two transition states for the OBJ parameters in $BzAr_n$ with $n=2-3,5$.

We will cite one other difference in the PES's. For $BzAr_4$ there exists a transition state which converges to a different minimum in one of the two downhill optimizations. For the OBJ parameters, the minima on either side of this transition state are $(3_c|1_c)$ and $(3_c|1|0)$. For the same transition state using the SCM parameters, the minima it connects are $(3_c|1_c)$ and $(4_s|0)$. If we follow the reaction pathway for these parameters we find that the $(3_c|1|0)$ structure is visited but it is not a stationary point and the optimization continues until the $(4_s|0)$ structure is reached.

In conclusion we find that as well as the variation in the energetic ordering of the stationary points, examples for which the OBJ and SCM PES's have other fundamental differences exist. However, these are rare, and it appears that even considerable changes in the LJ parameters leave the form of the stationary points largely unaffected. For brevity we have only tabulated a small fraction of the results we have obtained for the various stationary points.

2. $BzAr_{19}$

For $BzAr_{19}$, as for the smaller clusters, we study the effect of changing the LJ parameters on the underlying PES. The lowest minimum found, type $(7|5|7)$ (Fig. 3), is the same two-sided structure for both sets of LJ parameters. The Ar atoms do not completely surround the benzene molecule in this minimum, and there is partial ''solvation.'' We note that the $(l|m|n)$ notation is not able to describe the geometries for $BzAr_{19}$ as well as for the smaller clusters, but it can still be used to differentiate between one- and two-sided structures or structures involving bridging atoms. Also, unlike the descriptions of the smaller clusters, this notation no longer implies the existence of pseudo-planar arrangements of Ar atoms. Our lowest minimum has some residual double icosahedral structure for the Ar atoms, but much more icosahedral order is preserved in some higher energy minima (Fig. 4). The double icosahedron is the global minimum for Ar_{19} and when we add a benzene molecule the effect on the Ar atoms is reduced compared to smaller Ar_n clusters. Reordering is localized to Ar atoms in the vicinity of the benzene ring.

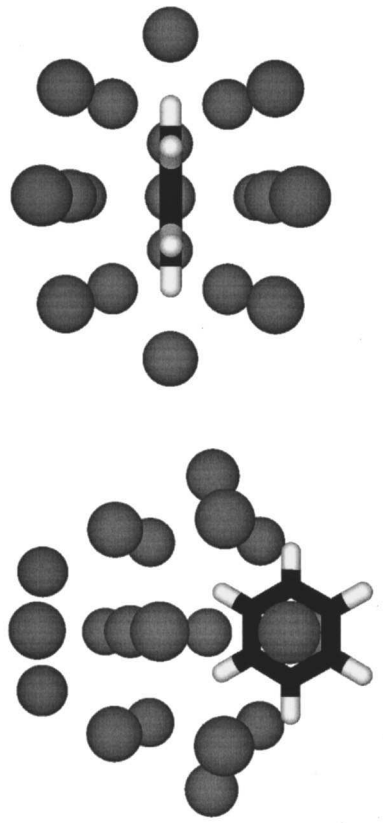

FIG. 3. Two views of the lowest energy $BzAr_{19}$ minimum found in the present study. The overall symmetry is C_{2v} and there is clearly some residual icosahedral structure.

Even though we find the same lowest energy minimum (aside from detailed bond lengths etc.) for both sets of LJ parameters there are important differences in the corresponding PES's. For the OBJ parameters two-sided structures dominate the lowest-lying minima. However, for the SCM parameters, although the lowest minimum is two-sided, there exists an energy range of about 0.4 millihartree (mh) above this structure in which we find only one-sided minima. Such differences in the PES's are likely to be of some importance when considering the dynamics of the system. We decided to use the SCM parameters for our Monte Carlo and molecular dynamics simulations as we prefer the larger Ar–Ar well depth and suspect that the smaller Ar–H well depth is more realistic. The experimental dissociation energy for $BzAr_1$ is 1.55 mh[44] which is closer to our SCM value of 1.72 mh than our OBJ value of 1.92 mh.

We start separate simulations from both the lowest-lying two-sided and one-sided minima located by systematic geometry optimisations from preliminary Monte Carlo simulations. These structures are shown in Figs. 3 and 4. Their binding energies are −39.04 mh and −38.90 mh, respec-

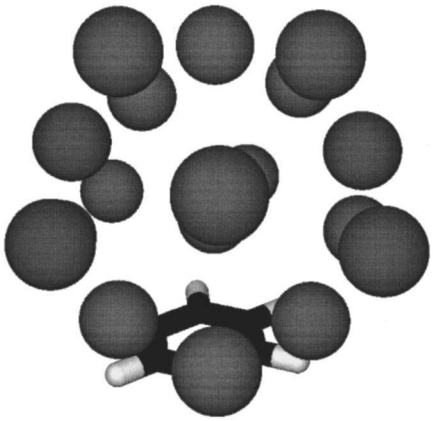

FIG. 4. The lowest energy one-sided minimum found for $BzAr_{19}$ in this study. The residual Ar_{19} double icosahedron can clearly be seen.

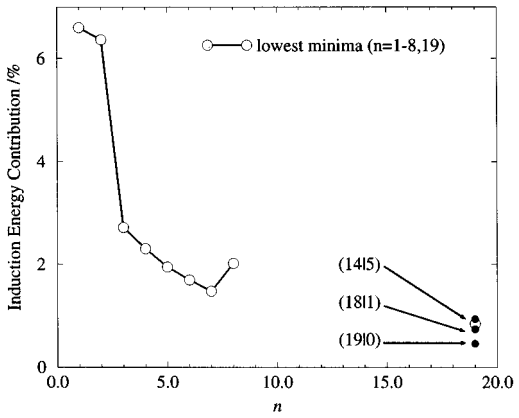

FIG. 5. The contribution of the induction energy in various $BzAr_n$ minima. The general trend is a decrease with increasing n, the increase at $n=8$ is due to the lowest minimum being two-sided for the first time for $n>2$. For $BzAr_{19}$ the induction contribution is always small, as many Ar atoms are in unfavourable positions with respect to the molecular quadrupole.

tively. Experimentally there appears to be no definitive conclusion regarding how these clusters form. There may be only one-sided structures initially, which then undergo solvation; alternatively both one-sided and two-sided structures may be formed so that both are observed spectroscopically. In fact, Adams and Stratt[8] have recently suggested that most $BzAr_n$ clusters formed in a jet are trapped in local minima in which the benzene molecule is bound to the surface of the Ar cluster. This argument is based upon new calculations of the benzene spectral shift which include the collective dielectric response of the cluster.[8] The suggestion that most benzene molecules are trapped in surface states contradicts the original conclusions of Guillaume *et al.*[3] which, however, have been revised in more recent work.[45]

B. The induction energy

We now investigate the effect of including the induction energy for the SCM LJ parameters. We find that apart from increasing the expense of the calculations, the PES's remain qualitatively unchanged to the extent that most minima look the same, and for $BzAr_n$ with $1 \leqslant n \leqslant 8,19$ the lowest-lying minima are effectively unchanged. Figure 5 shows the contribution of the induction energy for a selection of minima and the results are easy to interpret. The size of the induction energy contribution is mostly attributable to the location of the Ar atoms relative to the benzene quadrupole. An Ar atom above the C_6 axis of the benzene molecule will be most stabilised by the inclusion of the induction energy, whereas an atom lying in the plane of the molecule will be least stabilized. This follows from the properties of the quadrupole moment on the benzene molecule. The best illustration of this is for the simplest system, $BzAr_1$, for which there is just one rearrangement mechanism, involving the $(1_c|0)$ minimum and only one transition state, $(0|1|0)$, not counting permutational isomers. The minimum has C_{6v} symmetry, the Ar atom lying above the centre of the ring, and the transition state has C_{2v} symmetry with the Ar atom in the plane of the ring, equidistant from two adjacent H atoms. For the minimum the contribution of the induction energy to the total energy is 6.76%; for the transition state the contribution is only 0.680%.

We are now in a position to explain the results in Fig. 5. For $BzAr_2$, the induction energy contribution is also relatively high because the second Ar atom is situated directly below the centre of the benzene molecule, i.e. diametrically opposite the first Ar. The lowest minima found for $BzAr_3$ to $BzAr_7$ have smaller contributions as the positions of the Ar atoms are no longer optimal with respect to the molecular quadrupole moment, especially as they are all one-sided. The stabilization due to Ar–Ar dispersion interactions is proportionally greater than the change in the induction energy. At $BzAr_8$ we see an increase again—this is due to the global minimum being two-sided with one Ar atom on the C_6 axis below the benzene molecule, which is again an optimal position for stabilisation via the induction contribution.

For our $BzAr_{19}$ lowest minimum the contribution of the induction energy is only 0.849% because many of the Ar atoms are far from the C_6 axis of the benzene molecule. Our lowest lying (19|0) minimum has a 0.462% contribution, which is smaller because there is no Ar atom in an optimal position below the benzene molecule. We also found an (18|1) type structure with a contribution of 0.745%, and more fully ''solvated'' (14|5) minimum with a contribution of 0.940%—this structure has a more favourable arrangement of Ar atoms with respect to the molecular quadrupole moment.

For $BzAr_{19}$ the variation of the contribution of the induction energy with respect to the structure can be easily rationalized and it is always small (<1%). We use this argument to justify our neglect of the induction energy in subsequent Monte Carlo and molecular dynamics simulations, which run many times faster in this approximation.

C. Monte Carlo results

We start the simulation of $BzAr_{19}$ in the canonical ensemble using standard Metropolis Monte Carlo (MC) sam-

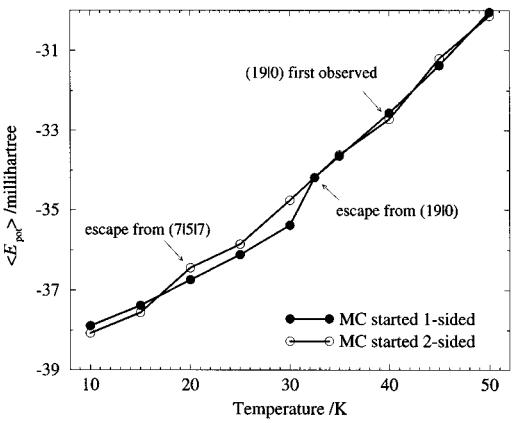

FIG. 6. Canonical caloric curves for $BzAr_{19}$ calculated from standard Metropolis Monte Carlo simulations with 10 million steps. The two runs were started from the lowest known one-sided and two-sided minima.

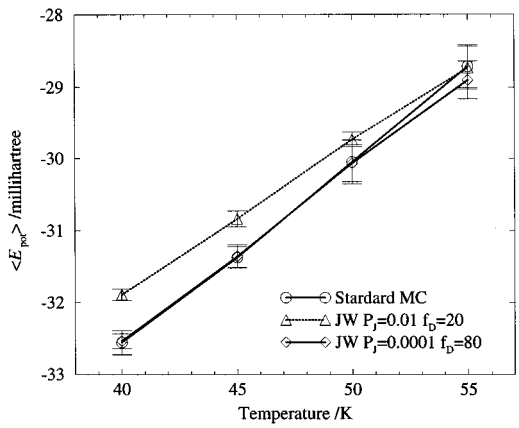

FIG. 7. Optimization of the Jump–walking parameters by comparison with well-converged standard Monte Carlo results at high temperatures. Jumping and diving very frequently leads to large correlation effects (Δ). Optimized Jump–walking parameters give the same results as standard Monte Carlo simulations at high temperatures because the full configurational space is accessible to both.

pling with 10 million steps at each temperature. The lowest one-sided minimum (19|0) and the lowest two-sided structure, (7|5|7), our lowest minimum, are used for the initial configuration in two separate runs. The resulting canonical caloric curves ($\langle E_{\rm pot}\rangle$ vs T) are shown in Fig. 6.

Although both caloric curves should represent the same ensemble they are inconsistent below about 32.5 K. The potential energy averages, $\langle E_{\rm pot}\rangle$, differ by up to 2% and both curves show kinks at different temperatures. A better understanding of these points can be achieved by periodic quenching of the Metropolis walker to a local minimum, following Stillinger and Weber.[46]

Each kink in the caloric curves corresponds to a first escape from a well-defined region of the PES, rather than a true melting process, indicating nonergodic behavior. For example, if we start from the one-sided (19|0) minimum then fully ''solvated'' two-sided structures are rarely sampled below 32.5 K although they are lower in energy. On the other hand, starting from the (7|5|7) minimum prevents the Metropolis walker from sampling any one-sided structures in simulations of this length up to 40 K although the associated region of configuration space is entropically significant. The only physical meaning that can be attached to the kinks in the caloric curves is the nonergodicity of these simulations and the presence of relatively high barriers between the minima. Adams and Stratt[7] observed similar restrictions in their MC simulations although they found transitions between the one-sided and the two-sided regimes at lower temperatures (below 30 K). This is not surprising because our SCM[1] potential parameters favour Ar–Ar binding compared to the OBJ[6]-type parameters used by Adams and Stratt.

We described in Sec. II C how the Jump–walking Monte Carlo technique (JW) helps to overcome high transition barriers in MC simulations. This method can produce results which are much more ergodic, especially at low temperatures. At high temperatures JW and standard MC should give the same thermodynamic averages because even the standard Metropolis walker is able to access the whole of configuration space in a reasonable number of steps.

We first concentrate on high temperature simulations between 40 K and 55 K to optimize the free parameters in our JW implementation, i.e., the jump-probability P_J, the dive-frequency f_D and the temperature difference ΔT between the parallel runs. Earlier studies[29] led us to set ΔT to 5 K which gives reasonable jump-acceptance rates of about 50%. P_J and f_D are more crucial in preventing correlation effects between the parallel runs. Figure 7 shows how severely the results are affected if the lower temperature Jumper follows the Diver too closely through configuration space, i.e. P_J is too high and/or f_D is too small. Here we also give the standard deviation of the mean potential energy to explain the poor convergence at 55 K. The container radius of 25 bohr in these runs was not optimal. Evaporation effects therefore disturbed the simulations making them less efficient. However, for temperatures below 55 K a large container size can be used without problems for simulations of this length.

We choose $P_J=0.0001$ and $f_D=80$ for our subsequent JW simulations. Accordingly, configurations stored by the Diver survive with a half-life of about 55 000 steps with a buffer file of 1000 entries. We equilibrate a buffer over about 150 000 steps before the Jumper starts. Then, if we use a 50% jump-acceptance rate, about 3 structures from the higher temperature run are used during each half-life period by the Jumper as new positions in configuration space. Ergodicity should be improved and indeed, the JW caloric curve in Fig. 8 differs from the standard MC results at lower temperatures (ΔT was set to 4 K below 30 K).

All kinks in the caloric curve disappear for the JW simulation. In particular, we cannot see any obvious feature in the JW caloric curve that could be interpreted as ''melting'' of the Ar_{19} cluster—simulations of neat Ar_{19} clusters exhibit solid/liquid coexistence between 26 K and 37 K in terms of a short-time-averaged order parameter.[47] There is no Van der Waals loop in the microcanonical caloric curve (presented below) because the potential energy cannot be used as an order parameter to distinguish between solidlike and liquid-

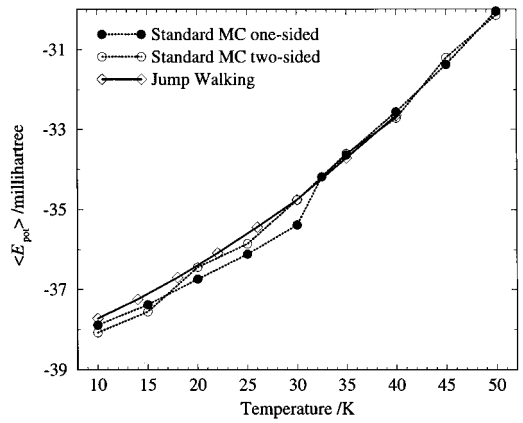

FIG. 8. Comparison of canonical caloric curves for $BzAr_{19}$ calculated with standard Metropolis Monte Carlo and Jump–walking. All kinks disappear in the more ergodic Jump–walking simulations.

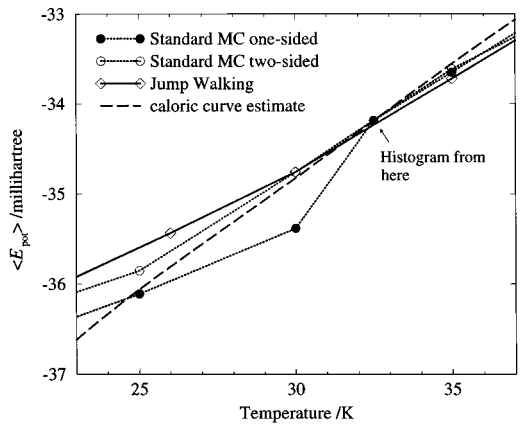

FIG. 9. Canonical caloric curve for $BzAr_{19}$ calculated with the single histogram method using the configurational number of states generated by an initially one-sided standard Monte Carlo run at 32.5 K. The curve interpolates the Jump–walking and the standard Monte Carlo results for a two-sided initial configuration at 30 K well.

like regions of phase space in this cluster.[48,49]

The utility of the more ergodic JW sampling technique is further illustrated if we use the relative configurational number of states, $\Omega_c(E_{\rm pot})\delta E_{\rm pot}$, from an initially one-sided standard MC simulation in the histogram method proposed by McDonald and Singer.[16] In Fig. 9 we show a canonical caloric curve calculated from the potential energy histogram generated at 32.5 K in an initially one-sided simulation, i.e., at a temperature just above the kink at about 30 K. It results in a smooth curve interpolating the results from JW and from initially two-sided standard MC simulations at 30 K quite well, despite the fact that we started from the (19|0) minimum. Two-sided configurations seem to dominate in this temperature range, although we find contributions from one-sided structures to the ensemble averages above 35 K in contrast to Adams and Stratt's[7] observations. As before, the latter discrepancy might be due to the differences in the potential parameters used. We obtained in our studies a variety of very low-lying one-sided minima (Sec. III A). However, we also use five times as many MC steps as Adams and Stratt and we show below that this is still insufficient to produce the correct transition barrier for the initially two-sided standard MC simulations.

In Fig. 10 we plot some caloric curves calculated from the configurational number of states obtained by single standard MC runs at various temperatures. As in Fig. 9 it is easy to see that the caloric curve calculated in this way is only accurate in the vicinity of the temperature at which the histogram was generated. This is expected, since a single temperature simulation cannot give accurate statistics at energies which are rarely sampled. Tsai and Jordan reached a similar conclusion in their studies of homogeneous systems.[29]

However, the results from the single histogram method help to explain systematic errors due to nonergodic sampling. In our simulations which are trapped in one-sided configurations below 32.5 K we obtain very different caloric curves from the configurational numbers of states calculated at 30 K and 32.5 (Fig. 10). The drop in the average potential energy at 30 K is not experienced by the more flexible Metropolis walker at 32.5 K which can sample a much bigger, less restricted configuration space. In contrast, the simulation at 30 K does not experience any contribution from two-sided structures which lie behind insurmountable barriers. The kink in the caloric curve from standard MC sampling started from the one-sided minimum has no other significance.

In simulations started from the two-sided minimum the caloric curves calculated by the histogram method exhibit a slightly different kind of discrepancy due to nonergodicity at 20 K and 40 K (Fig. 10). At 20 K, a temperature where nonergodic sampling is very likely, the Metropolis walker escapes from the (7|5|7) regime but still cannot sample the configuration space experienced by the run at 25 K. This is obvious since the calculated curves based on histograms collected at 25 K, 30 K and 35 K interpolate a lower lying potential energy average at 20 K. In contrast, the JW results presented in Fig. 8 imply that the standard MC sampling at 20 K represents the canonical ensemble quite well whereas the 25 K run seems to be trapped accidentally. The difference in interpretation is crucial for our MC simulations. The JW results suggest that larger standard MC runs are needed to improve convergence. However, if we try to elucidate the kink with the help of the single histogram method we find that the nonergodicity is due to insurmountable barriers. This problem can only be solved by systematic changes in approach such as JW Monte Carlo.

We now consider the results at 40 K, the lowest temperature where one-sided structures are observed in initially two-sided simulations of the given length. We can explain the small drop in the average potential energy if the one-sided regime becomes important entropically. However, the caloric curve obtained at 40 K is significantly worse than the curves from the neighboaring sampling points. On looking at the regions visited by the 40 K Metropolis walker using systematic quenching we found an unusual and accidental oversampling of one-sided structures compared to neighboring temperatures. The latter show one-sided structures only on a

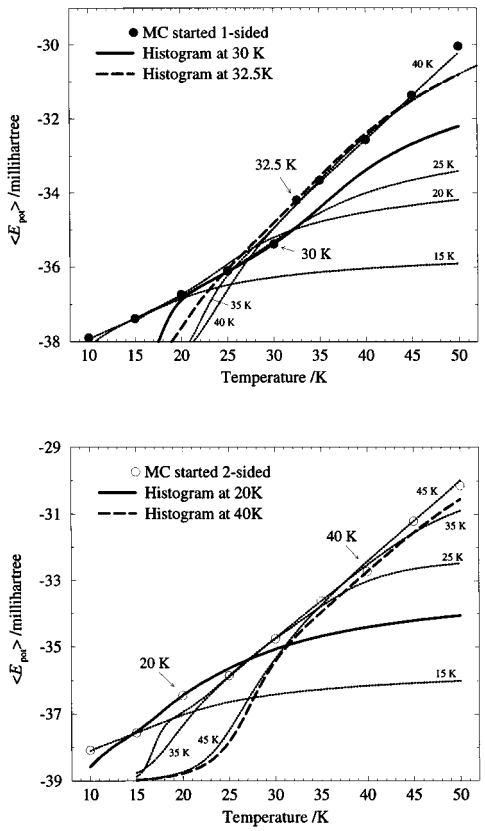

FIG. 10. Canonical caloric curves for $BzAr_{19}$ calculated with the single histogram method using configurational numbers of states derived from standard Metropolis Monte Carlo simulations at different temperatures. Top: Results for simulations started from a one-sided configuration. Bottom: Results for a two-sided starting point. We refer to these results in our examination of the systematic errors due to nonergodic sampling, in particular for the sampling temperatures emphasized by arrows. The dotted caloric curves correspond to various other temperatures.

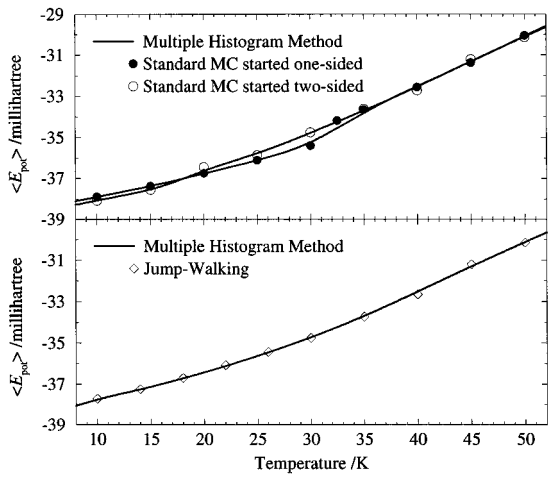

FIG. 11. Canonical caloric curves for $BzAr_{19}$ calculated with the multiple histogram method using configurational numbers of states derived from Monte Carlo simulations at different temperatures. Top: Multiple histogram results for standard Metropolic Monte Carlo simulations for both one-sided and two-sided starting configurations. Bottom: Results for Jump–walking Monte Carlo. The Jump–walking data for 45 K and 50 K are obtained from standard Metropolis sampling which coincides at these high temperatures.

smaller scale. The single histogram method helped us to find this inconsistency.

Finally, we employ a multiple histogram technique proposed by Weerasinghe and Amar[17] to combine the data gained from standard MC and from JW simulations (Fig. 11). Using the full histogram information results in smooth caloric curves which interpolate the discrete sampling points. Applying the convolution in Eq. 8 we calculate the relative number of states for an energy interval in phase space. Since we want to compare the resulting thermodynamic functions with our direct microcanonical simulations we take the integrals of motion corresponding to molecular dynamics into account [see Eq. (7)].

The absence of a Van der Waals loop in the corresponding microcanonical caloric curve (T vs E_{tot}, see Fig. 12) means that the canonical probability distribution of the total energy should be unimodal over the temperature range in question.[49] We come back to the microcanonical results in the next section. We also generate the corresponding canonical partition function to obtain thermodynamic functions in this ensemble [Eq. (11)]. Hence, we plot in Fig. 13 the canonical internal energy $U(T)$ due to Eq. 12. As expected, the functional shapes are very similar to the original caloric curves shown in Fig. 11.

We estimate the heat capacity $C_V(T)$ from the change in the internal energy $U(T)$ with respect to temperature [Eq. (13)]. Calculation of C_V from the potential energy fluctuations [Eq. (14)] results in almost perfectly matching curves in the given temperature interval. Therefore, numerical errors in the integration and differentiation routines for the thermodynamic functions can be neglected. We expect rather poor estimates around the lowest and the highest sampling points (10 K and 50 K) because of the missing information for neighboring temperatures (Fig. 14). In fact, we use additional standard Metropolis samplings at 5 K in the multiple histo-

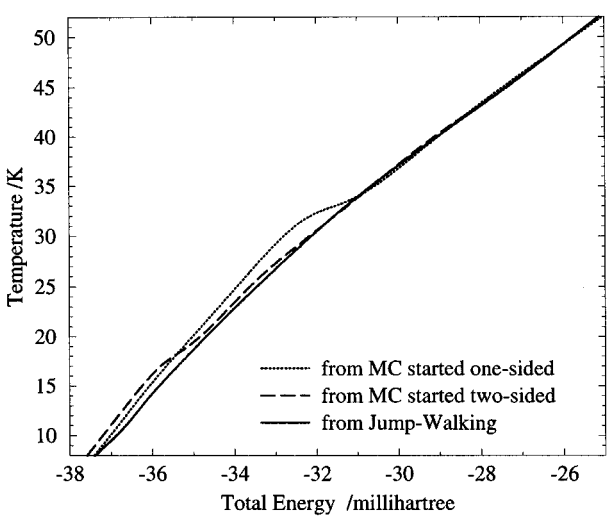

FIG. 12. Microcanonical caloric curves for $BzAr_{19}$ obtained from convolution of the configurational and kinetic number of states. The configurational contribution is generated by a multiple histogram method from standard Monte Carlo simulations.

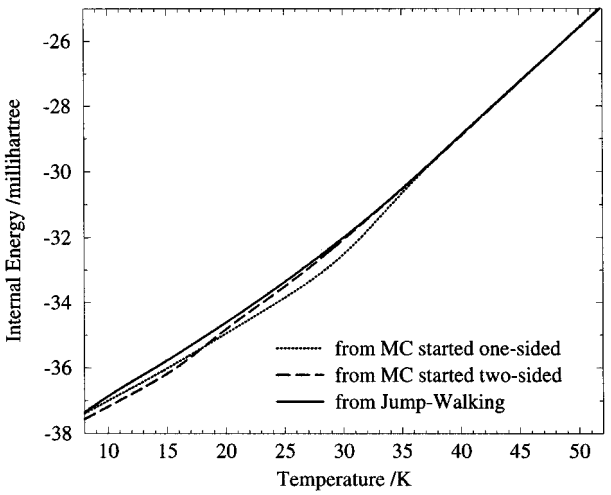

FIG. 13. Canonical internal Energy for $BzAr_{19}$ calculated after convolution of the configurational and kinetic number of states obtained from Monte Carlo simulations and analytical calculations. As expected, the functional shapes are very similar to the original caloric curves shown in Fig. 11.

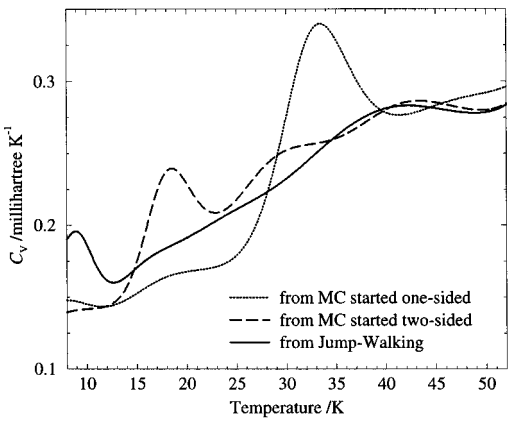

FIG. 14. Heat capacities for $BzAr_{19}$ calculated from the change in the canonical internal energy as a function of temperature. In contrast to standard Monte Carlo simulations Jump–walking results do not indicate a well-defined melting transition in this temperature range. The maximum at about 9 K in the curve obtained from Jump–walking is due to missing histogram information at 5 K for the Jump–walking results.

gram method for the one-sided and the two-sided results. However, we do not generate data at 5 K from Jump–walking Monte Carlo and a nonphysical maximum in the $C_V(T)$ curve remains at about 9 K. We obtained very similar errors for the standard MC results before we included the histograms generated at 5 K.

We did not investigate the possibility of multiple minima in Landau free energies or entropies to characterize melting in the present work.[48,50] To identify such features, if they exist, it would be necessary to invent an order parameter to distinguish between the solidlike and liquidlike parts of phase space.

D. Molecular dynamics results

Monte Carlo simulations which suffer from nonergodic sampling contain little physical meaning. In contrast, constant energy molecular dynamics (MD) simulations can associate real time scales with finite nonergodic trajectories restricted to well-defined regions of configuration space. To illustrate this we start with $BzAr_1$.

1. $BzAr_1$

The PES of $BzAr_1$ is very simple, there being only one minimum and one transition state. We use two approaches to estimate the rate at which the Ar atom crosses the plane of the benzene molecule, namely MD and the methods developed by Rice and Ramsperger, and Kassel[51] (RRK).

For MD, we use 43 ns trajectories with total energy between the energy of the transition state and the dissociation energy. Our MD results for $BzAr_{19}$ use the SCM parameters only but here we present, for comparison, those obtained with OBJ as well. At regular time intervals we analyse the Cartesian coordinates for all atoms in the system to determine which side of the ring the Ar atom is on and hence count the number of times the Ar atom crosses the ring. This leads directly to the side-crossing rate which converges well on the given time scale.

RRK theory assumes that the kinetic energy is accessible to all the vibrational normal modes in equal proportion. It can then be shown that the rate constant as a function of energy is

$$K(E)=\frac{h_{\mathrm{PG}}\Pi_{i=1}^{s}\nu_i}{h_{\mathrm{PG}}^{\dagger}\Pi_{i=1}^{s-1}\nu_i^{\dagger}}\left(\frac{E-E_{\mathrm{ts}}}{E}\right)^{s-1}, \tag{16}$$

where h_{PG} is the order of the point group; $\{\nu_i\}$, the normal mode frequencies; E, the energy measured from zero at the minimum; E_{ts}, the energy of the transition state and s is the number of vibrational degrees of freedom in the system, i.e., 3 for $BzAr_1$ with the benzene molecule considered rigid. The unlabelled quantities refer to the minimum; those labelled with †, to the transition state.

The results are plotted in Fig. 15 and show that the RRK results are always within one order of magnitude of those calculated from MD. The RRK results are translated such that the energy is zero at dissociation. Both the behavior at the transition state energies and close to dissociation are in quite good agreement.

We present these results for comparison with $BzAr_{19}$ for which we estimate barriers for one-sided to two-sided transitions from the MD trajectories. Calculating ring-crossing rates may not be as useful, as we have the possibility of multiple bridging atoms, and using RRK theory is tedious because of the number of transition states we would have to consider.

2. $BzAr_{19}$

In this section we study the escape of the $BzAr_{19}$ cluster from particular regions of configuration space and compare these to the Monte Carlo results. We start MD trajectories from the lowest known one-sided and two-sided structures in

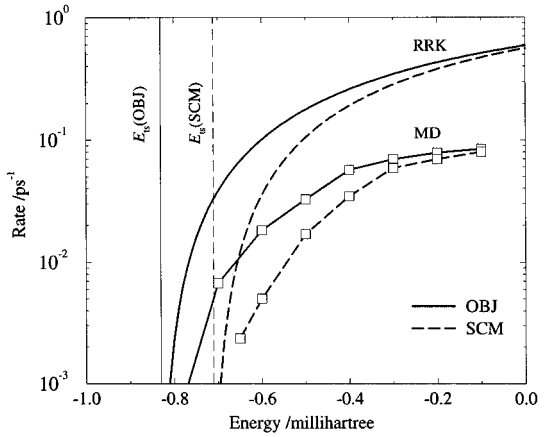

FIG. 15. Comparison of $BzAr_1$ ring-crossing rates from MD and RRK theory for both sets of Lennard-Jones parameters. All energies are measured relative to dissociation at zero and the transition state energies, E_{ts} are plotted as vertical lines to highlight the behaviour of the rate data.

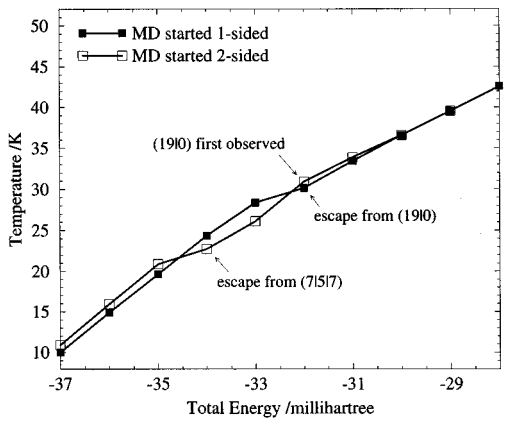

FIG. 16. Caloric curves for $BzAr_{19}$ calculated from molecular dynamics simulations of the microcanonical ensemble. The integration was initially started from both the lowest known one-sided and two-sided minima structures. Each kink in the resulting curves can be assigned to escape from particular regions of the configuration space, and is therefore due to kinetics rather than thermodynamics.

each case. We always use the final configuration at a given energy as the starting point for the next trajectory by rescaling the velocities to give a new kinetic energy. We loop over trajectories each of 10 ns length separated by 1 mh in total energy with the relative integration accuracy set to 5×10^{-6} for the conservation of energy. Fig. 16 shows the microcanonical caloric curves (T vs E_{tot}) produced by these simulations. Here the calculated kinetic temperature [Eq. (15)] is plotted against the total energy of the trajectory.

All the kinks in the caloric curves shown in Fig. 16 are symptomatic of escape from certain regions of configuration space, and therefore correspond to nonergodicity. These escapes are actually of significance in finite time scale experiments.

We find that an average kinetic temperature of about 23 K is needed to escape from the (7|5|7) starting structure on the time scale of our simulations. This corresponds to 5 mh (1100 cm^{-1}) total energy above the -39 mh energy of the (7|5|7) minimum. Consequently, the first kink in the two-sided curve in Fig. 16 is assigned to escape from the (7|5|7) minimum. We expect that this kink corresponds to the ''melting'' point Fried and Mukamel[4] found in their studies of $BzAr_{16}$ and $BzAr_{21}$ at about 20 K. As in earlier work we considered the Lindemann criterion,[4,47,52] i.e., the relative rms fluctuation of the Van der Waals bond lengths. We observed the same clear indication of a ''melting'' process due to the Lindemann criterion as seen by Fried and Mukamel in their studies and in contrast to the heat capacity results shown in Fig. 14. However, for all other kinks in the caloric curve the Lindemann criterion does not appear to be meaningful and we do not consider it further in the present work.

The experimentally more important threshold between the one-sided and the two-sided regime appears at higher energy. At a kinetic temperature of about 30 K (corresponding to 7 mh or 1500 cm^{-1}) the (19|0) structure changes for the first time to one which is two-sided in our simulation. This energy difference is equivalent to about fifty times the energy gap of 0.14 mh (31 cm^{-1}) between the lowest lying one-sided and two-sided minima. The two-sided trajectory consistently becomes one-sided first at about 30 K on our time scale. It is noteworthy that both regimes are entropically important at higher temperatures. Both one-sided and two-sided structures are visited in all of our simulations above 30 K. These results confirm the expectations from Fried and Mukamel's[4] studies of $BzAr_{16}$ and $BzAr_{21}$ but disagree with the observations of Adams and Stratt[7] for $BzAr_{19}$. In the latter MD studies ring crossing was not observed up to 30 K. We observe side-crossing at temperatures below 30 K. This discrepancy is rather surprising since we use a potential parameter set which favors Ar–Ar binding compared to the OBJ-like parameters that Adams and Stratt and Fried and Mukamel used (Sec. III A). However, our results support the more recent suggestion of Adams and Stratt that below about 30 K the benzene chromophore might be kinetically trapped in a surface state for significant periods of time.[8]

It is very difficult to decide what time scales are appropriate in the related experiments.[5,4,7] We do not observe a one-sided/two-sided transition during the 10 ns simulation time at 33 mh, i.e. 6 mh (1300 cm^{-1}) above the lowest minimum. This energy is slightly below our first estimate of the barrier height. However, if we integrate a longer trajectory (43 ns) we find first one or two Ar atoms occasionally migrating to the initially non-occupied side but coming back to the main Ar cluster on a very short time scale. After about 26 ns fully ''solvated'' two-sided structures occur but it also happens quite often that all Ar atoms come together on one side again. We believe the one-sided/two-sided transition barrier is very close to this energy, and it is noteworthy that MD provided a good estimate of the transition barrier in $BzAr_1$ (Fig. 15).

A more detailed study of the above feature would involve calculating the rearrangement pathways and the corresponding rate constants. However, we choose not to persue this point further in the present paper.

Our MC and the MD results are compared in Fig. 17;

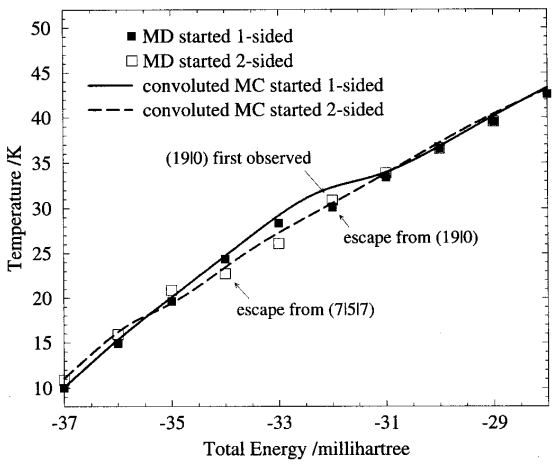

FIG. 17. Microcanonical caloric curves for $BzAr_{19}$ calculated from canonical standard Monte Carlo samplings and direct molecular dynamic simulation of the microcanonical ensemble. Structural transitions occur at similar temperatures in both methods.

they match quite well despite the fact that the results pertain to different ensembles. It is interesting that escape from particular regions of configuration space, a symptom of nonergodicity, happens at rather similar points in MC and MD except for the sampling of the one-sided regime in initially two-sided standard Monte Carlo simulations. The latter inconsistency probably arises because the number of MC steps was too small to sample all regions of configuration space accessible at this temperature. In simulations at 37.5 K with 20 million MC steps we did indeed observe some configurations belonging to the one-sided regime.

The coincidence of the other kinks gives us some confidence that the escape times found in the MD simulations could be experimentally significant. If both MD and MC simulations fail to find structural interconversions it seems unlikely that alternative escape-routes exist. For the one-sided/two-sided transition the fact that MD trajectories starting at very different points produce the same estimate of the escape temperature is probably significant.

IV. CONCLUSIONS

We have shown, with examples, how the potential energy surfaces of $BzAr_n$ clusters may vary with changes in the Lennard-Jones parameters. For smaller n our surveys are quite systematic because low energy minima can be predicted due to the large influence the benzene molecule has on the ordering of the Ar atoms, and there are only a few degrees of freedom. For $BzAr_{19}$ we have discussed only general differences in the lower-lying minima and found that the lowest energy minima found in numerous Monte Carlo and molecular dynamics simulations are qualitatively the same for the two sets of parameters. We have also shown that the induction energy has little influence on the form of the potential energy surfaces and that its importance is reduced as n increases. For $BzAr_{19}$ we neglect this contribution to the energy for the purpose of simulations as it constitutes $<1\%$ of the total energy.

In the simulation of the canonical and the microcanonical ensembles we have shown how severely thermodynamic averages are affected by nonergodic sampling. We combined the standard Monte Carlo method with the more ergodic Jump–walking sampling and a histogram method to obtain a better understanding of the underlying nonergodicity. Our implementation of Jump–walking minimises correlation effects and storage problems. We find that the Jump–walking approach provides much better sampling of configuration space. The ''melting'' process in $BzAr_{19}$ does not produce a clear feature in the canonical caloric curve.

We also employed a multiple histogram method and numerical convolution to generate the relative number of states in phase space in order to calculate thermodynamic functions in the canonical and the microcanonical ensembles. The numerical operations are accurate and the results for the microcanonical ensemble match well with estimates from direct MD simulations.

For describing finite timescale experiments more insight might be gained from molecular dynamics simulations. For the important one-sided/two-sided transition the MC and MD results provide a consistent picture in which to estimate transition barriers and escape times. We employed the Bulirsch-Stoer integration scheme to integrate the MD trajectories. In general, for each kink in the canonical and the microcanonical caloric curve, signifying non-ergodicity, we are able to assign escape from a particular region of configuration space consistent with both MC and MD simulations. Our results suggest that $BzAr_n$ clusters produced by pick-up experiments are likely to be found with the benzene molecule in a surface site on a timescale of tens of nanoseconds at temperatures below around 30 K, providing some support for the recent interpretation of spectra by Adams and Stratt in terms of ''nonwetting'' isomers.[8]

ACKNOWLEDGMENTS

A. D. is a scholar of the Studienstiftung des Deutschen Volkes and a Marie Curie Fellow of the European Union. M.P.H. gratefully acknowledges financial support from the EPSRC and D.J.W. from the Royal Society. We are also grateful to Mr. Mark Miller for providing the least-squares fitting program.

[1] M. Schmidt, J. Le Calvé, and M. Mons, J. Chem. Phys. **98**, 6102 (1993).
[2] D. J. Wales, Mol. Phys. **74**, 1 (1991).
[3] C. Guillaume, M. Mons, J. Le Calvé, and I. Dimicoli, J. Chem. Phys. **97**, 5193 (1993).
[4] L. E. Fried and S. Mukamel, J. Chem. Phys. **96**, 116 (1992).
[5] J. Bösiger, R. Knochenmuss, and S. Leutwyler, Phys. Rev. Lett. **62**, 3058 (1989).
[6] M. J. Ondrechen, Z. Berkovitch-Yellin, and J. Jortner, J. Am. Chem. Soc. **103**, 6586 (1981).
[7] J. E. Adams and R. M. Stratt, J. Chem. Phys. **93**, 1358 (1990).
[8] J. E. Adams and R. M. Stratt, J. Chem. Phys. **105**, 1743 (1996).
[9] P. L. A. Popelier, A. J. Stone, and D. J. Wales, Faraday Discuss. **97**, 243 (1994).

[10] D. J. Wales, P. L. A. Popelier, and A. J. Stone, J. Chem. Phys. **102**, 5551 (1995).
[11] D. J. Wales, A. J. Stone, and P. L. A. Popelier, Chem. Phys. Lett. **240**, 89 (1995).
[12] M. Y. Hahn and L. Whetten, Phys. Rev. Lett. **61**, 1190 (1988).
[13] A. J. Stone, Chem. Phys. Lett. **83**, 233 (1981).
[14] A. J. Stone and M. Alderton, Mol. Phys. **56**, 1047 (1985).
[15] D. D. Frantz, D. L. Freeman, and J. D. Doll, J. Chem. Phys. **93**, 2769 (1990).
[16] I. R. McDonald and K. Singer, Faraday Discuss. Chem. Soc. **43**, 40 (1967).
[17] S. Weerasinghe and F. G. Amar, J. Chem. Phys. **98**, 4967 (1993).
[18] J. E. Jones and A. E. Ingham, Proc. R. Soc. London, Ser. A **107**, 636 (1925).
[19] A. J. Stone, *The Theory of Intermolecular Forces* (Oxford University Press, Oxford 1996).
[20] R. Krishnan, J. S. Binkley, R. Seeger, and J. A. Pople, J. Chem. Phys. **72**, 650 (1980).
[21] C. M. Møller and M. S. Plesset, Phys. Rev. **46**, 618 (1934).
[22] Landolt-Börnstein, *Zahlenwerte und Funktionen* (Springer, Berlin 1951), Vol. 1, p. 510.
[23] C. G. Gray and K. E. Gubbins, *Theory of Molecular Fluids* (Clarendon, Oxford 1984), Vol. 1 p. 577.
[24] C. J. Cerjan and W. H. Miller, J. Chem. Phys. **75**, 2800 (1981); J. Simons, P. Jørgenson, H. Tayler, and J. Ozment, J. Phys. Chem. **87**, 2745 (1983); D. O'Neal, H. Taylor, and J. Simons, *ibid.* **88**, 1510 (1984); J. Baker, J. Comput. Chem. **7**, 385 (1986); **8**, 563 (1987).
[25] J. N. Murrel and K. J. Laidler, Trans. Faraday Soc. **64**, 371 (1968).
[26] D. J. Wales, J. Chem. Phys. **101**, 3750 (1994).
[27] A. J. Stone, A. Dullweber, M. P. Hodges, P. L. A. Popelier, and D. J. Wales, ORIENT: A program for studying interactions between molecules *Version 3.2* (University of Cambridge, 1995), available at: http://fandango.ch.cam.ac.uk.
[28] N. Metropolis, A. W. Rosenbluth, M. N. Rosenbluth, A. H. Teller, and E. Teller, J. Chem. Phys. **21**, 1087 (1953).
[29] C. J. Tsai and K. D. Jordan, J. Chem. Phys. **99**, 6957 (1993).
[30] A. Matro, D. L. Freeman, and R. Q. Topper, J. Chem. Phys. **104**, 8690 (1996).
[31] A. M. Ferrenberg and R. H. Swendsen, Phys. Rev. Lett. **61**, 2635 (1988).
[32] A. M. Ferrenberg and R. H. Swendsen, Phys. Rev. Lett. **63**, 1195 (1989).
[33] C. Bichara, J.-P. Gaspard, and J.-C. Mathieu, Phys. Lett. A **119**, 462 (1987).
[34] F. Calvo and P. Labastie, Chem. Phys. Lett. **247**, 395 (1995).
[35] M. Toda, R. Kubo, and N. Saitô, *Statistical Physics I* (Springer-Verlag, Berlin, Heidelberg, 1992).
[36] P. Labastie and R. L. Whetten, Phys. Rev. Lett. **65**, 1567 (1990).
[37] M. P. Allen and D. J. Tildesley, *Computer Simulation of Liquids* (Clarendon, Oxford 1987).
[38] J. Stoer and R. Bulirsch, *Introduction to Numerical Analysis* (Springer-Verlag, New York 1980).
[39] W. H. Press, S. A. Teukolsky, W. T. Vettering, and B. P. Flannery, *Numerical Recipes* (Cambridge University Press, Cambridge 1992).
[40] T. Çağin and J. R. Ray, Phys. Rev. A **37**, 247 (1988).
[41] D. J. Evans, Molec. Phys. **34**, 317 (1977).
[42] D. J. Evans and S. Murad, Mol. Phys. **34**, 327 (1977).
[43] R. M. Lynden-Bell and A. J. Stone, Mol. Sim. **3**, 271 (1989).
[44] H. Krause and H. J. Neusser, J. Chem. Phys. **99**, 6278 (1993).
[45] C. Guillaume, J. Le Calvé, I. Dimicoli, and M. Mons, J. Chim. Phys. Phys.-Chim. Biol. **92**, 334 (1995).
[46] F. H. Stillinger and T. A. Weber, Phys. Rev. A **25**, 978 (1982).
[47] T. L. Beck, J. Jellinek, and R. S. Berry, J. Chem. Phys. **87**, 545 (1987).
[48] R. M. Lynden-Bell and D. J. Wales, J. Chem. Phys. **101**, 1460 (1994).
[49] D. J. Wales and J. P. K. Doye, J. Chem. Phys. **103**, 3061 (1995); D. J. Wales and R. S. Berry, Phys. Rev. Lett. **73**, 2875 (1994); D. J. Wales and J. P. K. Doye, in *Large Clusters of Atoms and Molecules*, edited by T. P. Martin, NATA ASI Series E (1995), p. 241.
[50] J. P. K. Doye and D. J. Wales, J. Chem. Phys. **102**, 9673 (1995).
[51] O. K. Rice and R. C. Ramsberger, J. Am. Chem. Soc. **49**, 1616 (1927); **50**, 617 (1928); L. S. Kassel, J. Phys. Chem. **32**, 225 (1928); K. J. Laidler, *Chemical Kinetics* (Harper Collins, New York, 1987).
[52] F. A. Lindemann, Phys. Z. **11**, 609 (1910); Engineering **94**, 515 (1912).